ASME Journal of Tribology
Online journal at:
https://asmedigitalcollection.asme.org/tribology

Pär Nyman
Propulsion Development,
Scania CV AB R&D,
Building 117-12,
Södertälje 151 87, Sweden
e-mail: par.nyman@nynas.com

Peter Björklund
Materials Technology,
Scania CV AB R&D,
Building 101-2,
Södertälje 151 87, Sweden
e-mail: peter_x.bjorklund@scania.com

Negin Yaghini
Materials Technology,
Scania CV AB R&D,
Building 101-2,
Södertälje 151 87, Sweden
e-mail: negin.yaghini@scania.com

Li Lu
School of Pharmacy,
The University of Nottingham,
University Park Campus,
Nottingham NG7 2RD, UK
e-mail: li.lu1@nottingham.ac.uk

Elizabeth R. Hopper
Lubrizol Ltd.,
The Knowle, Nether Lane Hazelwood,
Derbyshire DE56 4AN, UK
e-mail: elizabeth.hopper@lubrizol.com

Gregory Hunt[1]
Lubrizol Ltd.,
The Knowle, Nether Lane Hazelwood,
Derbyshire DE56 4AN, UK
e-mail: gregory.hunt@lubrizol.com

Investigating the Failure Mechanism of Wet eMachines in the Presence of Transmission Oils

This paper investigates the failure mechanisms in electric machines used in heavy trucks and buses exposed to transmission oil. Five machines from field operations were examined. Subsystem tests—copper corrosion testing, conductive deposit tests, material compatibility tests, and oil analysis—were conducted. Copper sulfide, known for its conductive properties, was found in failed machines and during subsystem tests with lubricants containing reactive sulfur components in contact with exposed copper. Two prerequisites for the chemical reaction—the presence of reagents and sufficient activation energy—were met at normal operating temperatures. Analysis revealed the sulfur presence in damaged machines and identified cracks in the polymer coating on copper wires, allowing corrosive substances to reach the copper surface. The proposed failure mechanism involves active sulfur reacting with copper to form copper sulfide. These layers can create contact bridges between phases in the eMachine, leading to short circuits, sharp temperature increases, electrical arcing, and total machine failure. Coating aging experiments showed that fluids can form conductive films on the polymer layer. Oil conductivity measurements showed minor changes within the static dissipative regime, and contamination by transmission and axle oil elements was found in failed eMachines but not in functional ones. Activation energy experiments demonstrated that copper sulfide forms at normal operating temperatures, with damage likely within 10–100 days depending on conditions. These findings highlight the risks associated with certain oils in eMachines and the need for further research to develop strategies to mitigate these risks and ensure long-term reliability. [DOI: 10.1115/1.4067832]

Keywords: coatings, corrosion, electrical contacts, lubricant additives, lubricants, polymeric additives, soft materials, surface properties and characterization

1 Introduction

In an electric vehicle, the energy generated by fuel cells or stored in batteries is converted into mechanical energy through one or more electric machines (eMachines). These eMachines are comprised of a rotor and a stator. The stator generates the electromagnetic field, while the rotor converts the electromagnetic field into rotational motion. The stator is made up of copper wires, also known as hair pins due to their shape. These copper wires are arranged in such a way that they form three continuous winding phases, creating electromagnetic coils. Although there are other winding geometries, this study focuses on the hair pin design. The rotor, on the other hand, consists of permanent or electromagnets stacked on iron sheets and mounted on a shaft supported by bearings at each end. By switching the electric phases on and off in a predetermined sequence, the magnetic field can be rotated, causing the magnets on the rotor to rotate as well. Typically, the rotor shaft is connected to the input shaft of the transmission.

Hair pin windings in eMachines typically have a polymer coating providing electrical insulation. These thin coatings are selected based on their electrical, thermal, and mechanical properties and as such enable a wide range of polymers for use in these applications. The coating thickness can be made from single or multiple polymers. Where the coating is removed to enable welding, a remedial process is applied to re-cover the copper and provide electrical insulation again. This is typically performed on the stator end windings.

Even though eMachines have high efficiency, they require cooling typically by allowing fluid to pass through the system transporting heat away. Cooling can be either direct or indirect. In direct

[1]Corresponding author.

Contributed by the Tribology Division of ASME for publication in the Journal of Tribology. Manuscript received October 27, 2024; final manuscript received February 4, 2025; published online February 24, 2025. Assoc. Editor: Oliver Koch.

cooling, the cooling fluid is in direct contact with the eMachine or heat source. In indirect cooling, the fluid is transferred from the heat source to the coolant through another solid body. This study applies to direct cooled systems or systems with combinations of indirect and direct cooling, a so-called wet eMachine. In wet eMachines, the coolant fluid is in contact with the stator end windings. This enables efficient cooling but places some requirements on the fluid used. It must not be conductive or corrosive toward copper.

In heavy electric vehicles, the eMachine's rotor is rotating much faster than the wheels of that vehicle. Therefore, a transmission is required to overcome the rotational speed difference. The transmission contains gears and bearings that require cooling and lubrication. Combining the need for cooling the stator and lubricating the transmission would enable the overall system to be designed in a compact manner.

Traditional lubricants such as axle oils, manual transmission fluid, and automatic transmission fluid, provide good wear and scuffing protection [1,2]. The protection of gear and bearing surfaces in transmissions against scuffing wear and seizure is provided by the extreme pressure (EP) additives that are constituents of the transmission oils [3–5]. EP-additives consist of sulfur-rich chemically reactive molecules. They function by forming low shear resistance layers consisting of iron sulfide [4]. This process has much in common with the formation of corrosion layers on copper surfaces at the high temperatures generated by the eMachines where the sulfur-containing EP-additives react with the copper surfaces to form copper sulfide layers.

Recently, lubricants have been developed which have sufficient wear and scuffing performance and excellent copper corrosion performance in addition to compatibility with the wire coatings in wet eMachines (Fig. 1). These fluids contain low sulfur concentrations and are known as eFluids [6,7].

Earlier studies [6] have shown that there is a difference in corrosion rate depending on whether the copper is immersed in oil, here referred as to the liquid phase, or if the corrosion occurs above the surface in the presence of corrosive vapor from the oil, here referred to as the vapor phase.

In this paper, we attempt to explain the chain of events leading to damages such as those shown in Fig. 2.

The proposed hypothesis is that corrosive sulfur-containing EP-additives react with the copper in the hair pins to form copper sulfide. These copper sulfide layers have been shown to have conductive properties [8,9], which means that if the corrosion layers are allowed to grow, a contact bridge between the phases of the eMachine can form. This leads to a short circuit followed by sharp temperature increase resulting in electrical arcing and subsequent melting of components in the eMachine leading to a total breakdown and the eMachine needs to be replaced (Fig. 3).

For chemical reactions, in this case, corrosion, to initiate, two criteria must be fulfilled: the presence of reagents and sufficient activation energy for the reaction to take place. For this application, there needs to be reactive sulfur species present such as those found in EP-additives of transmission and axle oils. The sulfur species must also be able to reach the nascent copper surface and finally for this to lead to a short circuit this must take place in the vicinity of a neighboring phase lead closing the connection between two electrical circuits.

2 Materials and Methods

2.1 eMachine Failure Analysis. Five eMachine stators from buses in customer operation in Sweden, Spain, and Norway have been analyzed. Optical images were obtained using an AxioZoom V16 from Carl Zeiss with the ZENCORE software.

Samples from the polymer coatings and deposits from damaged areas at the welding side of the stator were collected. Elemental analysis was carried out by scanning electron microscopy (SEM) using a Zeiss 360 FE-SEM with energy dispersive X-ray spectroscopy (EDS) using an Oxford Ultim Max detector with an accelerating voltage of 20 kV.

Lubricating fluid samples were collected for analysis from each of the eMachines before disassembly. The elemental content of the fluids collected from the vehicles was analyzed using inductively coupled plasma optical emission spectrometry according to ASTM D5185 for phosphorus, calcium, and copper concentrations, and using energy dispersive X-ray fluorescence spectrometry according to ASTM D7751 for sulfur concentration.

Analysis of the eMachine temperatures using a sensor placed close to the end windings shows that the normal operating temperature lies between 80 °C and 100 °C, and never exceeds 125 °C.

2.2 Subsystem Testing

2.2.1 Wire Corrosion Test. The effects of EP chemistry at concentration ranges from 0.05 wt% to 10 wt% in PAO4 were compared using the wire corrosion test (WCT) in both the solution and vapor phases. The WCT was performed as outlined by Hunt et al. [10]. Approximately 1 m long and 64 μm diameter two pure copper (99.99 wt%) wires were used. One was suspended in 400 $\pm$ 1 ml of test lubricant (liquid) and the other is fixed above the test lubricant (vapor). A direct current of 1 mA was applied to

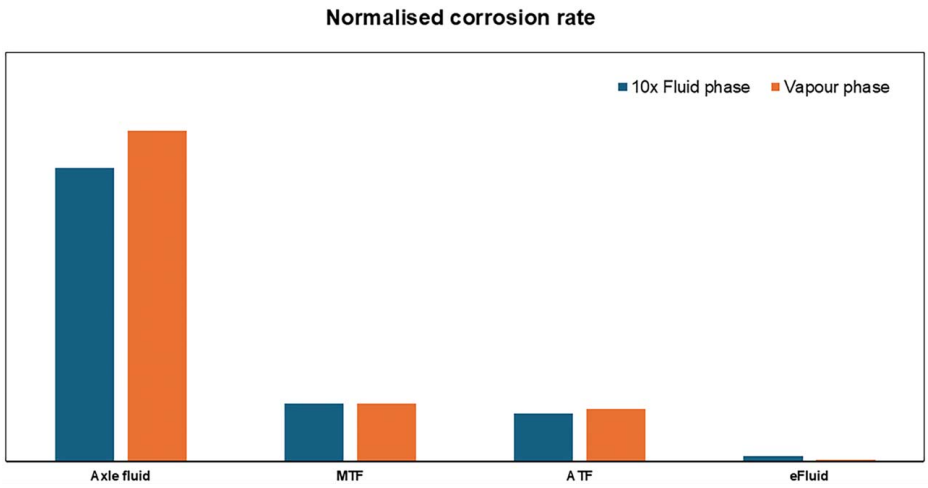

Fig. 1 Normalized relative corrosion rates between some common transmission and axle lubricants (reproduced with permission from Ref. [6]). N.B. The liquid phase here is referred to as the fluid phase.

Fig. 2 Stator with severe damage

each wire. The lubricant is held to ±0.25 °C of the desired test temperature by means of a thermostatically controlled heating oil bath. The resistance at the start of test is used to normalize the difference in length of the wire, with the calculated value compared to the normalized length. Resistivity changes with temperature and this is accounted for through various equations allowing results to be normalized. Comparisons of corrosion reactions at different temperatures can, therefore, be attributed directly to the corrosion process [11]. The change in resistance is used to calculate the apparent change in the wire radius.

2.2.1.1 Kinetic analysis of the corrosion process. Reaction kinetics can often be expressed based on the Arrhenius law [12] (Eq. (1))

$$k(T) = A\exp\left(-\frac{E_a}{RT}\right) \tag{1}$$

where A is the pre-exponential factor, R is the universal gas constant equal to 8.314 J/mol/K, E_a is the activation energy (kJ/mol), and $k(T)$ is the Arrhenius equation constant which depends on the temperature (T). The temperature dependence of a reaction can be fit by the simple Arrhenius law. By rearranging the law into Eq. (2)

$$\ln k = \ln A - \frac{E_a}{RT} \tag{2}$$

A plot of ln k as a function of $1/T$ should therefore yield a straight line whose slope is $-E_a/R$ and whose intercept is ln A. The determination of the Arrhenius activation energy allows us to interpret the rate of change of the equilibrium reaction rate with temperature in terms of the distribution of reaction energies when the reaction proceeds at equilibrium at a given temperature.

The Eyring equation [13,14], which is similar to the Arrhenius equation but is more applicable to solution phase reactions and is derived from statistical thermodynamics, is a useful method to describe the relationship between reaction rate and temperature (Eq. (3))

$$k = \frac{k_B T}{h} e^{-\left(\frac{\Delta H^{\ddagger}}{RT}\right)} e^{\left(\frac{\Delta S^{\ddagger}}{R}\right)} \tag{3}$$

where k is the equilibrium constant, and k_B is the Boltzmann constant 1.381×10^{-23} J/K, T is the absolute temperature in Kelvin, h is the Planck's constant, 6.626×10^{-34} Js, $\Delta H^{\ddagger}$ is the enthalpy of activation, R is the universal gas constant, 8.314 J/mol/K, and $\Delta S^{\ddagger}$ is the entropy of activation. The values of $\Delta H^{\ddagger}$, and a y-intercept $\left(\frac{\Delta S^{\ddagger}}{R}\right) + \ln\frac{k_B}{h}$ and $\Delta S^{\ddagger}$ can be obtained from a plot of ln k/T versus $1/T$. Where the equation is a straight line with a negative slope, $\left(\frac{\Delta H^{\ddagger}}{RT}\right)$, and a y-intercept $\left(\frac{\Delta S^{\ddagger}}{R}\right) + \ln\frac{k_B}{h}$.

2.2.2 Conductive Deposit Test. The effect of the axle oil and the eFluid on the formation of conductive deposits was assessed using the conductive deposit test (CDT) [15]. The test was carried out as outlined by Hunt et al. [16]. 225 ± 4 g of lubricant and a scaffold containing two printed circuit board (PCB) stacks are added to a 1 L neck glass reactor vessel. The lower PCB stack is submerged in the test lubricant, while the other is held above. A power supply of +5 V DC, with up to 200 mA current is applied to a single board in each stack. The glassware is then assembled and heated in an oven for 500 h at 150 °C. A condenser connected to the sealed reactor vessel is setup outside of the oven to contain oil vapors in the vapor phase. The setup is schematically depicted in Fig. 4. Multiple PCBs are used for each phase and are spaced 1 mm apart in a stack.

The interdigitated copper finger design of the PCB, with a comb-type pattern like the IPC-TM-650 [17] for the copper electrode is shown in Fig. 4 (right). Each PCB board contains 28.3 g of copper on a glass fiber-epoxy substrate. In this study, only the two PCB boards in the middle of the stacks, for vapor and liquid phases, were energized with a constant voltage for the duration of the test. This new conductive layer deposit test provides insight into the formation of conductive deposits in both vapor and liquid phases simultaneously and in situ. The test directly monitors the formation of conducting deposits in real-time and the growth of deposit formation during the end of the test period.

2.2.3 Coated Wires Aging. The effects of a traditional axle fluid, an eFluid, and two sulfur-containing fluids were compared on sections of polymer-coated wires (copper—4 × 2 mm coated

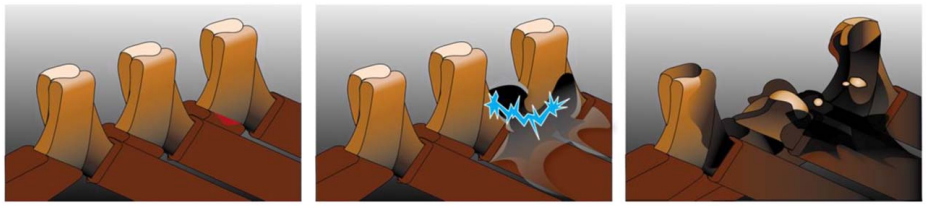

Fig. 3 Graphic showing the evolution of stator end winding failure

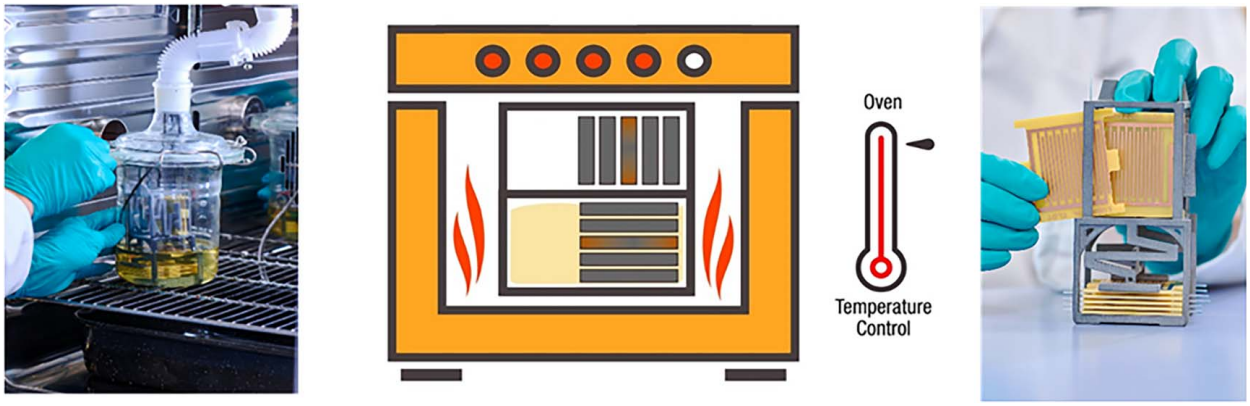

Fig. 4 Schematic of the CDT. The edges of the PCB boards are shown: horizontal is the liquid phase and vertical is the vapor phase. Center boards are energized (Reproduced with permission from Ref. [15]).

with ~150 μm thick polymer). The axle fluid contained both active sulfur and high concentrations of phosphates and phosphites. Two formulations containing only base fluid and EP chemistry were also used: one with low active sulfur and one with high active sulfur concentrations. The eFluid contains no active sulfur or phosphorus species, but sulfur is present in the form of sulfonates.

To age polymer-coated wires, two configurations were used: in one case straight sections of wire were half immersed in fluid in a beaker, and in the other wires were bent into a U-shape and the bend immersed in fluid in a beaker with the ends pointing into the vapor phase. The beakers were covered with foil and held in an oven at 150 °C for 500 h or 1000 h. At the end of the test, the wires were removed and rinsed with SBP2L, a solvent comprised of C6 to C10 paraffins and cycloparaffins with low levels of aromatics and used as purchased from Shell.

SEM and corresponding EDS data were collected using a Phenom XL benchtop SEM, operated at 15 kV and 60 Pa atmospheric pressure. Optical images were obtained using an Olympus SZX10 stereomicroscope.

To analyze the top ~10 nm of the surface, X-ray Photoelectron Spectroscopy (XPS) data were collected using a Thermo Fisher *K-α* photoelectron spectrometer equipped with a monochromatic Al *Kα* X-ray source (1486.8 eV) and analyzed using CasaXPS [18]. The X-ray source was operated at 2.5 mA emission current and 12 kV anode bias. The spot was an elliptical shape with a long axis of 400 μm. A flood gun was used to mitigate sample charging, with an emission current of 150 μA. The spectra were calibrated by setting the C 1s peak to 284.8 eV. Survey scans were collected between 1350 eV and −10 eV binding energy, with 160 eV pass energy, step size 0.5 eV, and dwell time 150 ms. High-resolution scans were collected over an appropriate energy range at 20 eV pass energy, step size 0.1 eV, and dwell time 1500 ms for S 2p and P 2p where appropriate. Atomic concentrations at the surface were determined using the survey scans, and accurate peak positions were obtained from the high-resolution scans.

Time-of-flight secondary ion mass spectrometry (TOF-SIMS) depth profiling was performed using a TOF-SIMS V (IONTOF GmbH). The dual-beam mode was employed to analyze an area of $150 \times 150\ \mu m^2$ using a 25 keV Bi_3^+ liquid metal ion gun at the center of a $300 \times 300\ \mu m^2$ sputter crater formed by a 10 keV Ar_{1600}^+ gas cluster ion beam delivering 10 nA. A low-energy (21 eV) electron flood gun was applied for charge compensation. A depth profile was measured for each sample. The process consisted of repeated cycles involving both analysis and sputtering. In each cycle, a liquid metal ion gun was used to collect surface species information, followed by sputtering with a gas cluster ion beam to remove the sample material. This sequence was repeated to build up a depth profile of the sample. The depth profile measurement was conducted in non-interlaced mode with three sputter frames per cycle, one analysis scan per cycle, and a pause time of 2.0 s between cycles. The end of the measurement varied across samples and was determined when the polymer ion changes became stable and reached the polymer layer. The secondary ions produced include positive ions, negative ions, and neutrals. These ions are then selected and analyzed by the mass analyzer in separate polarity modes. Data for each sample were collected in both polarities (positive and negative) with a 200 μs cycle time of the TOF mass analyzer (mass range of *m/z* 0–3677). Data acquisition and analysis were performed using SurfaceLab 7.4 (IONTOF GmbH), and all peak intensities were normalized to total ion counts. The depth of the $300 \times 300\ \mu$m crater from the low active sulfur aged sample (produced after 3203 s of sputter time in TOF-SIMS depth profile analysis) was measured using a Zeta Optical Profiler. The measurement was conducted with a *z* range set to 68 μm and a step number of 200 (step size 0.343 μm). The average height at the center of the crater was measured as 35.72 μm, giving a sputter rate of approximately 11 nm/s.

The conductivity of the wires was measured using a Megger MIT2500 surface insulation resistance device at 100 V. Conductivity of the fluids was measured using a Scientifica conductivity meter model 627. The elemental content of the fluids after aging was analyzed following ASTM D5185.

2.2.4 eMachine Stator Deposits. Samples from deposits under the coating and the surface of copper wires from the eMachine were analyzed by TOF-SIMS. To remove the excess oil, the deposits were heat treated in a Thermogravimetric Analysis (TGA) instrument at 210 °C for 20 h prior to the analysis. The particles were fixed on a silicon substrate and analyzed in an M6 TOF-SIMS instrument (IONTOF GmbH). Argon cluster ions were used for sputter cleaning (10 keV Ar2000+, $600 \times 600\ \mu m^2$, 10 nA, 45 s for one area, and 280 s for two other areas), removing up to approximately 1–1.5 μm of organic material on the sample surface. The depth of the crater has not been measured since the depth of the sputter craters is expected to be small relative to the unevenness of the surface topography. Surface imaging analysis ($350 \times 350\ \mu m^2$) of the sputter-cleaned areas was performed using 30 keV Bi3 + primary ions.

3 Results and Discussion

3.1 Motor Failure Analysis. Five eMachine stators from buses in customer operation in Sweden, Spain, and Norway have been analyzed. Four of these, units 1–4, have been reported to have electrical issues and short-circuiting between 120,000 km and 400,000 km. The damage severity differed between the units, one (unit 2) showing only a small dark spot in the end winding, and other three showing very severe breakdown with large pieces of copper missing (e.g., Fig. 2). In all cases, the damages occurred

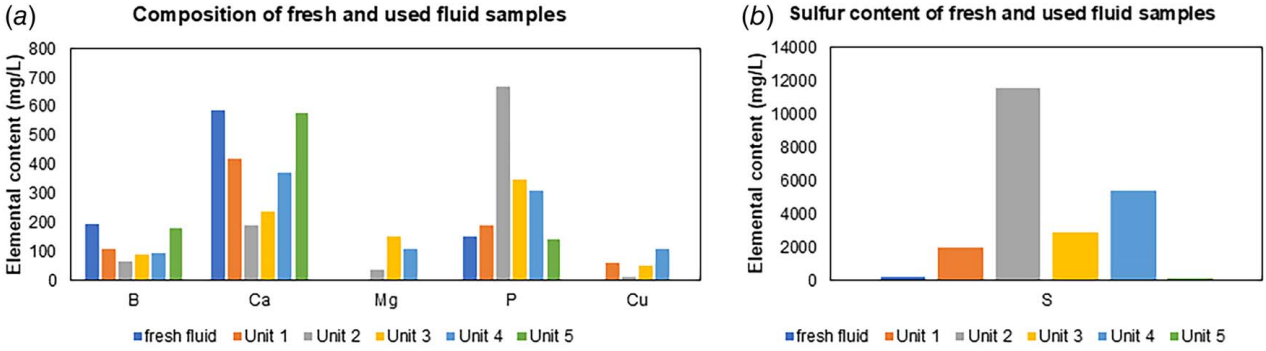

Fig. 5 Elemental levels in fresh and used fluid samples: (*a*) composition of fresh and used fluid samples and (*b*) sulfur content of fresh and used fluid samples

on the side of the stator where the hair pins are welded together. Two stators showed damage far above the nominal oil level and two showed damage approximately at the nominal oil level. Unit 5 had no reports of any failure in operation and visual inspection showed no signs of corrosion at disassembly at 168,000 km.

All buses were operated in similar duty cycles, the major difference where the ambient temperatures. As expected, vehicles operated in Spain see higher ambient temperatures than those in Sweden and Norway. However, temperature readouts from sensors placed inside eMachine windings show similar temperature distribution for all five vehicles showing that the differences in damage seen are not related to differences in operating conditions.

Fluid samples from the four damaged units show altered levels of elements typical for transmission and axle oils (boron, calcium, magnesium, phosphorus, and sulfur, Fig. 5). All four damaged eMachines contain relatively high amounts of sulfur, indicating transmission or axle oil contamination in the eMachine cooling circuit, most likely a result of a top-up with the wrong oils at the workshop. N.B. The units are most likely not contaminated with the same transmission or axle oil. Unit 5 showed a slight decrease in additive elements including sulfur. Depletion of additive components is not unusual for oils in use.

Some copper was present in the fluid samples from units 1–4, indicating the presence of corrosion. Unit 5 showed no signs of elevated copper levels.

Copper is normally not found in transmission oils when new, so elevated copper levels in the oil samples indicate the presence of corrosion. Optical microscopy was used to locate cracks in the polymer layers on the units with no or less severe damage, units 2 and 5. In units with severe short-circuiting, units 1, 3, and 4, the temperatures reached were high enough to melt copper, so there is no way of knowing if the polymer cracking occurred before or after the short circuit. Several locations were found with cracks, insufficient coating coverage, poor resin adhesion, and other damage to the coating layer (Figs. 6 and 7).

For units 1, 3, and 4, the damage was more severe (Fig. 8). Samples of deposits were taken from the coating (sample A) and on the surface of copper wires (sample B), and elemental analysis was performed by SEM–EDS. EDS (Fig. 9) confirms the presence of copper, sulfur, carbon, calcium, and oxygen.

Carbon was found in high concentrations, likely residues of burnt polymer and/or transmission or axle oil as a result from the extremely high temperatures. Elemental mapping showed that copper and sulfur were found in the same regions (Fig. 9). Note that some variations in intensity arise due to the topography of the sample. In the area with high copper and sulfur, the ratio of the copper to sulfur varies from 1:1 to 2:1, however, due to the high roughness of the sample and unknown thickness of the corrosion products this quantification is not conclusive, since the EDS measurement depth may extend to metallic copper below [19].

Samples from deposits under the coating and the surface of copper wires were analyzed by TOF-SIMS. Copper sulfides were clearly identified as a major component, by the observation of several Cu_xS_y cluster ions in the negative TOF-SIMS spectra after sputter cleaning (Fig. 10). The cluster ions were identified based

Fig. 6 Crack on the polymer coating close to the weld area in unit 2

Fig. 7 Cracks in the insulation layers in unit 5

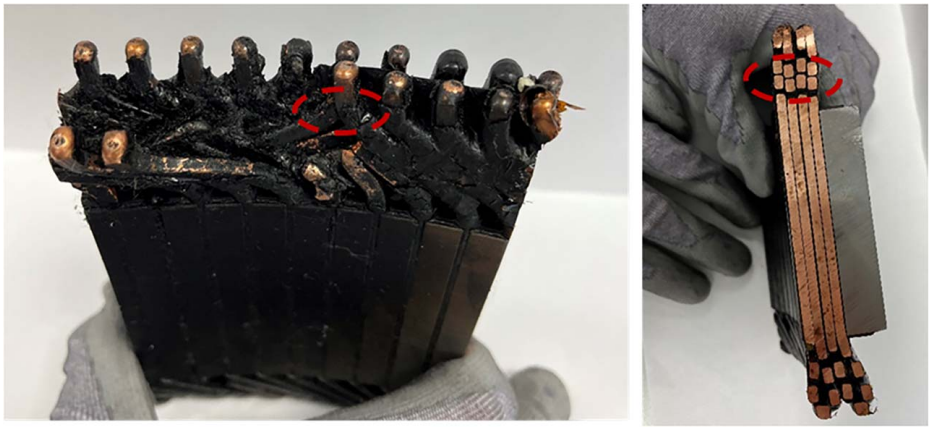

Fig. 8 Failed eMachine unit: (left) cross section of the stator (sample A) and (right) damaged area on the welding side of the eMachine (sample B). The regions where samples were collected are marked with dashed lines.

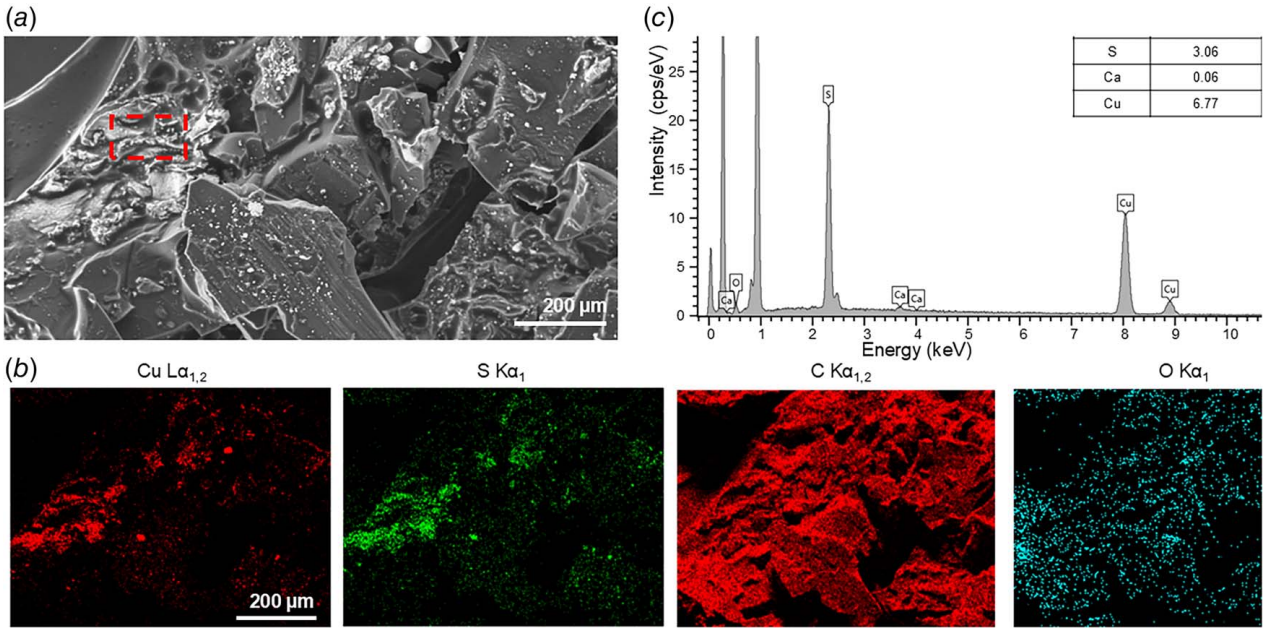

Fig. 9 The remaining polymer layer on the welding side (sample A): (*a*) SEM image, (*b*) SEM–EDS maps for copper, sulfur, carbon, and oxygen, and (*c*) composition within the dashed box

on detailed agreement between the observed peak positions (m/z) and theoretical mass values (within 0.01–0.02 u), as well as agreement between observed peak intensity distributions and theoretical isotope distributions (Fig. 11). Cu_xS_y cluster ions are detected in the TOF-SIMS spectra of all three areas, strongly indicating the presence of copper sulfides in the sample deposits.

The intensity distribution between Cu_xS_y clusters can be used to obtain the stoichiometry ratio of copper sulfide. However, a complementary analysis of reference samples with different Cu/S stoichiometries is needed to validate the ratio.

3.2 Subsystem Testing

3.2.1 Wire Corrosion Test. The function of long-duration high-temperature corrosion testing is to provide information about lubricant compatibility and corrosion performance of in-service lubricants. This approach is appropriate only if the same corrosion process occurs at the elevated temperature and is not affected by new or competing reactions that are only viable at the elevated temperature. The rate information collected here can be used to provide an understanding of the temperature dependency of the active sulfur chemistry reaction with copper to form a copper sulfide adduct. To test the effect of active sulfur concentration on the rate of corrosion, a series of dilutions of active sulfur chemistry were performed. Dibutylpolysulfide was added at varying concentrations [5]. The results are shown in Fig. 12.

The rate of corrosion increases with increased concentration in a linear manner at 130 °C and 150 °C. The vapor phase reaction in both cases possesses an increased rate of reaction versus that of the liquid phase. In all cases, the reactions are likely first-order processes. Equation (4) outlines the most likely reaction process occurring.

$$Cu + S \rightarrow CuS \tag{4}$$

The experimentally determined activation energies [13] for both vapor and liquid phases are 82 kJ/mol and 86 kJ/mol, respectively. The vapor and liquid phase activation energies are in good

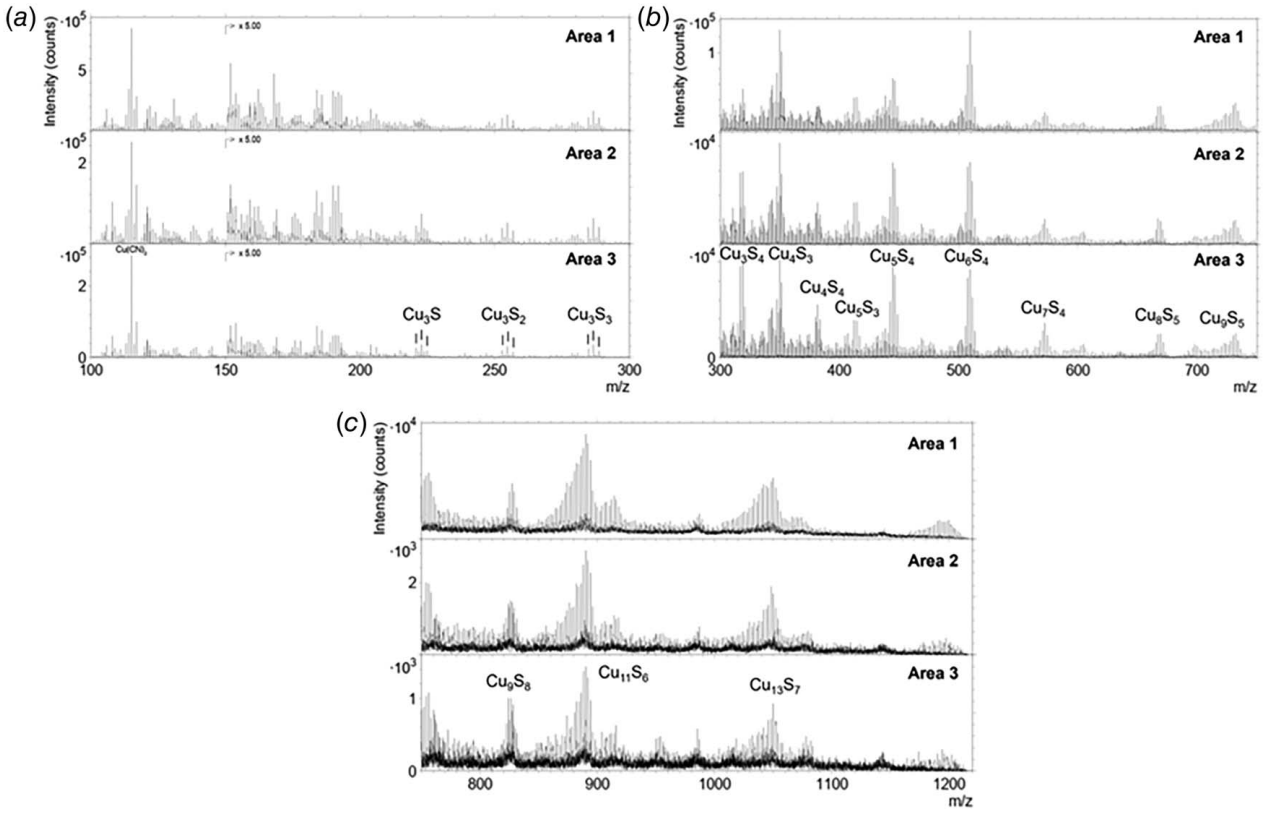

Fig. 10 TOF-SIMS spectra for three samples of deposits under the coating of a failed eMachine, showing the Cu_xS_y cluster ions in the negative ion spectra with adjusted intensity for *m/z* range (*a*) 100–300, (*b*) 300–800, and (*c*) 800–1200

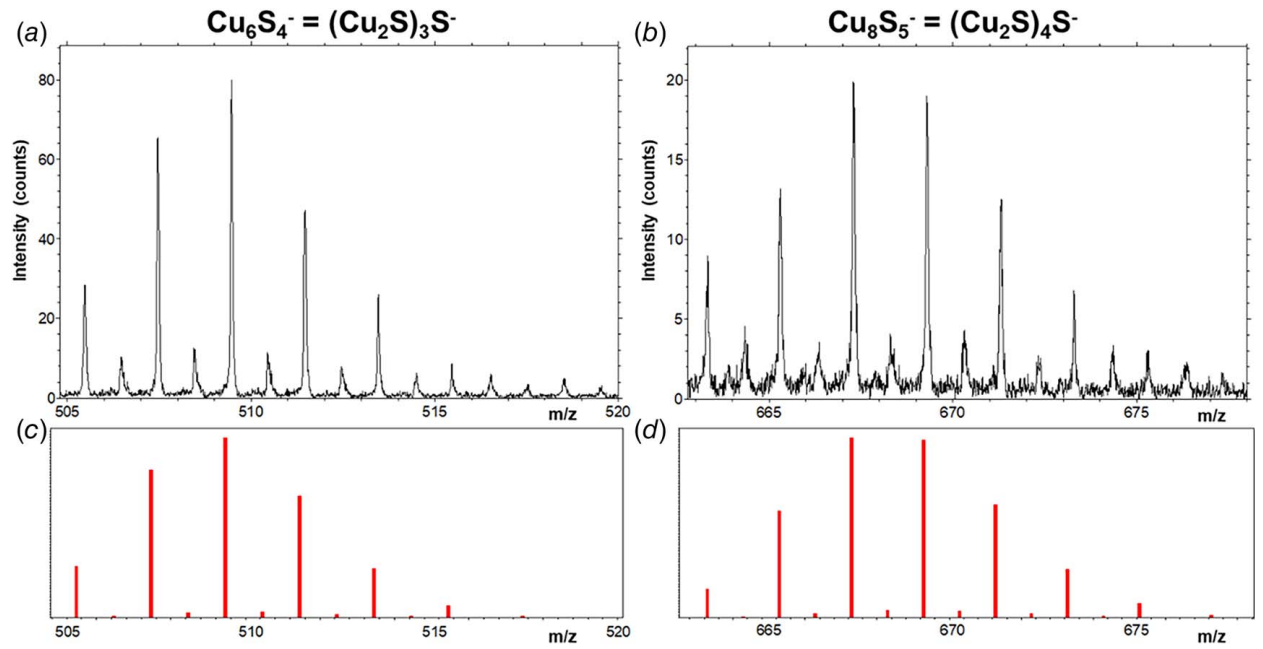

Fig. 11 Comparison between (*a*) and (*b*) measured peak positions (*m/z*) for two example clusters; and (c) and (*d*) the corresponding theoretical mass values for copper sulfide ion clusters

agreement with each other suggesting the same reaction process is occurring in both liquid and vapor phases, with the vapor phase having a slightly lower activation energy. The activation energy of 82–86 kJ/mol indicates that this process is not spontaneous and requires a thermal event to start the reaction. It is worth noting that having the same activation energy does not mean the rate of corrosion will be the same in both phases. In this case, the vapor phase has an increased corrosion rate (Fig. 13). To estimate the reaction rate at actual motor temperatures, the use of half-life calculations is used. In chemical kinetics, the half-life of a reaction is the time taken for the concentration of a substance to fall to half its initial concentration. Assuming the reaction remains first order,

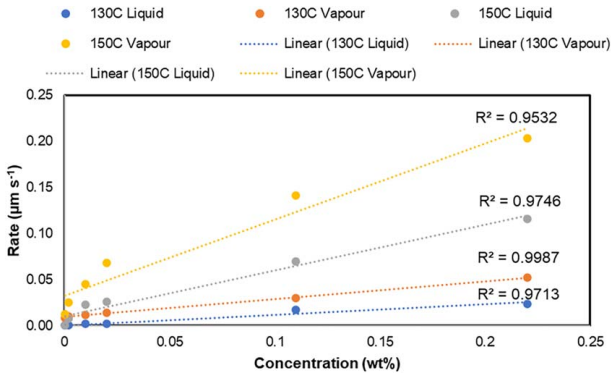

Fig. 12 Plot of rate versus concentration indicating a pseudo-first-order plot for the corrosion of copper in the presence of active sulfur concentration at 130 °C and 150 °C in both liquid and vapor phases

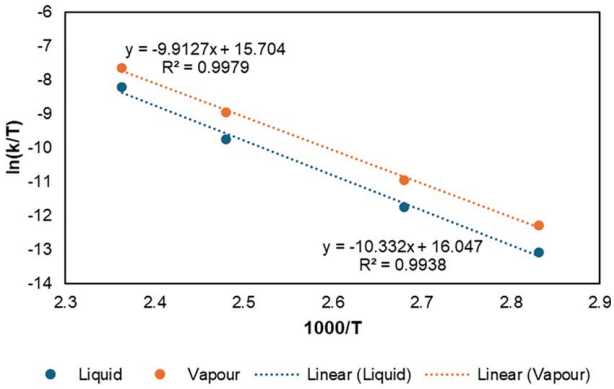

Fig. 13 Eyring plot for liquid and vapor phase EP chemistry reactions at 100–150 °C

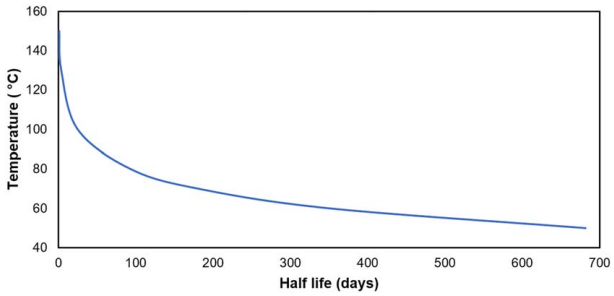

Fig. 14 Plot of temperature versus calculated half-life for the reaction in Eq. (4) based upon the kinetics from the Eyring plot in Fig. 13

then the comparison of the half-life at different temperatures can be calculated. Figure 14 shows the calculated half-life for the first-order reaction in Eq. (4).

3.2.2 Conductive Deposit Test. To test the conductivity of the corrosion deposits of the axle and eFluid samples, the conductive deposit test was performed at 150 °C for 500 h. Optical images of the end of test boards are shown in Fig. 15. The axle fluid produced conductive deposits in both the liquid and vapor phases after 150 h. The optical image of the boards shows a black deposit across the board surface. The axle fluid vapor phase PCBs show an increase in conductance after 72 h reaching 1.0×10^{-4} S with the conductance increasing slightly to 1.2×10^{-4} S. after 500 h. The axle fluid liquid phase indicated an increase in conductance after 110 h, reaching 1.4×10^{-4} S. The conductance continued to increase up to 500 h reaching 2.8×10^{-3} S. Conductive deposits were formed in both the liquid and vapor phases.

The eFluid shows no change in conductance in the vapor or liquid phases, with no evidence for the formation of a conductive deposit. The conductance did not change throughout the duration of the test and remained at the minimum conductance value measurable at 100 V DC throughout the 500 h test.

3.2.3 Coated Wires Aging. To test the effects of lubricants on polymer-coated wires, several aging tests were conducted. Wires were half immersed in the liquid phase in two configurations: in one case the wires were bent into a U-shape and the bend immersed in liquid with the ends pointing into the vapor phase, allowing measurements of the effect of the fluid on only the coating. In the other case, straight sections of wire were half immersed with exposed copper at both ends, allowing the effect of exposed copper to be determined. The beakers were covered and held in an oven at 150 °C for 500 h or 1000 h. At the end of the test, the wires were removed and rinsed.

3.2.3.1 Appearance of the wires post-test. After aging, discoloration was seen on all wires (Figs. 16 and 17). The fresh polymer coating appeared pink in color and turned gray after 500 h of aging in the air. When wires were aged in eFluid, the coating aged in the vapor phase turned gray, while in the liquid phase the fluid protected the immersed section of coated wire from discoloration slightly, after both 500 h and 1000 h, leaving a pink/gray color. Using the low active sulfur fluid, a brown deposit was formed on only the immersed section of coating. The top layer of deposit was easily brushed off the surface when touched, and the lower levels could be scratched off to reveal the gray coating. For the high active sulfur fluid and axle fluid, a black deposit was formed in the liquid phase, and brown coloring was seen in the vapor phase. The deposit from the axle fluid appeared shiny and bumpy in places after both 500 h and 1000 h (Fig. 17).

3.2.3.2 Conductivity of the wires and coatings. Before aging, the wires were conductive through the length of the copper and the polymer coating was completely insulative (resistance > 20 GΩ) both when measured from the polymer coating surface to the end of the copper wire, and when measured between two points on the polymer surface. After aging, all wires (both bent and straight) remained conductive through the length of the copper.

All coatings remained insulative when the conductivity was measured through the polymer to the wire (i.e., from the surface of the polymer coating to the end of the exposed copper), although the resistance values decreased to 1–10 GΩ. The polymer coating is, therefore, intact, and continues to protect the copper wire. However, the black deposits from aging in axle fluid, particularly the bubbled regions, were found to be conductive when measured along the surface, with resistance values around 5–20 MΩ. One conductive area was also found on the deposit from the high active sulfur fluid.

3.2.3.3 Effect of exposed copper in the fluid. The effect of the fluid on the exposed copper was determined from the aged straight wires. In most cases, when copper was exposed both in the liquid and vapor phases it appeared black after aging, however, the copper exposed in eFluid appeared unchanged, indicating good copper corrosion prevention properties of the eFluid. When copper was exposed in the liquid phase in high active sulfur fluid and axle fluid, a solid mass of decomposition products formed outside the end of the wire (Fig. 18(*a*)). SEM–EDS showed that these solids both contained carbon, oxygen, copper, and sulfur, and in the deposit from the wire aged in axle fluid phosphorus was also present (Fig. 18(*b*)).

When the solid was snapped off the end of the wire aged in axle fluid (liquid phase), the copper wire was found to be solid

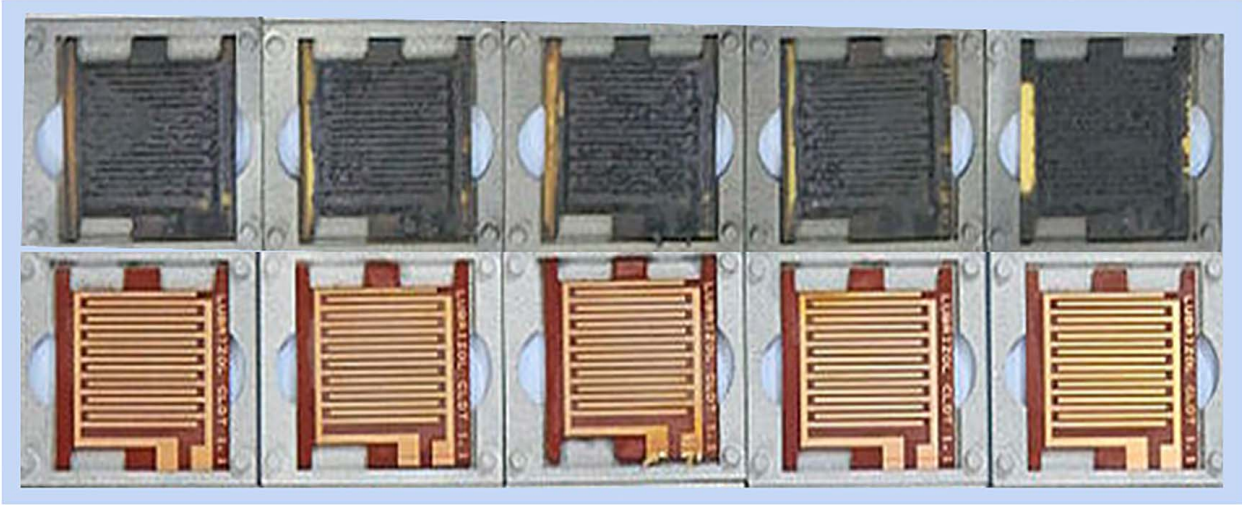

Fig. 15 Optical images of the liquid phase conductive deposit boards after 500 h exposure to (top) axle fluid and (bottom) eFluid

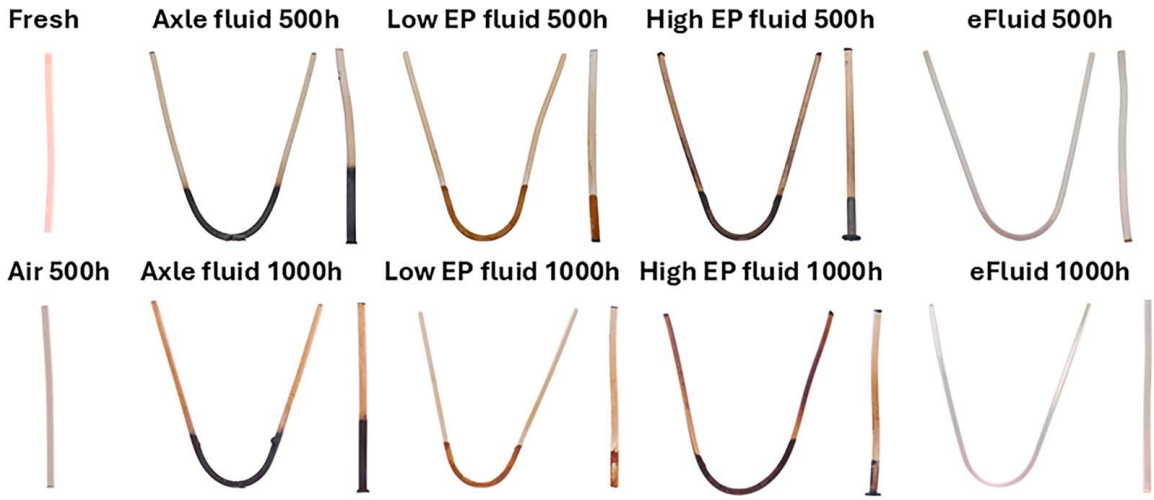

Fig. 16 Appearance of polymer-coated wires aged in various fluids

and blackened beneath a gray and intact coating (Fig. 18(*c*)). When the deposit was removed from the wire aged in high active sulfur fluid, the coating was visibly gray and still intact, however, the copper wire had been damaged for about 2 mm within the coating, leaving a black solid that crumbled when probed (Fig. 18(*c*)). The copper has likely reacted with sulfur in the fluid to form copper sulfide, removing copper from the wire itself. Conversely, the deposit from the axle fluid did not consume as much copper and only contained 1.3% copper (compared with 5.1% from the high active sulfur fluid) and 2.4% sulfur (compared with 5.0%). Instead, the deposit contained phosphorus and higher levels of oxygen, possibly phosphates or phosphites deposited from the fluid.

3.2.3.4 Composition of deposits on the coating surface. To assess the composition of the deposits on the coating surfaces after aging, XPS (Fig. 19) and SEM–EDS were used. The results from only the straight wires are presented here for simplicity but are similar to those from the bent wires.

By XPS, the top surface (~10 nm) of the deposit could be analyzed, whereas SEM–EDS has a higher penetration depth (>1 μm). The trends seen by each technique were in agreement.

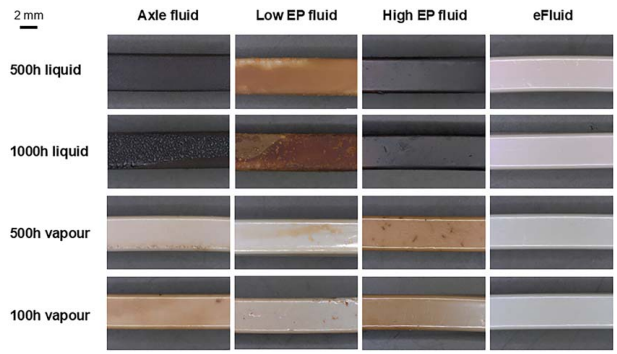

Fig. 17 Representative magnified appearance of polymer-coated wires aged in various fluids, shown for the straight wires

The fresh coating contains primarily carbon and oxygen, with trace amounts of other elements (sodium, zinc, calcium, nitrogen, and sulfur) present. After aging in the air for 500 h, the oxygen concentration increased from 5.3% to 17.3%, and the concentrations of sodium, calcium, and sulfur increased (0.24–0.58%, 0.33–1.89%,

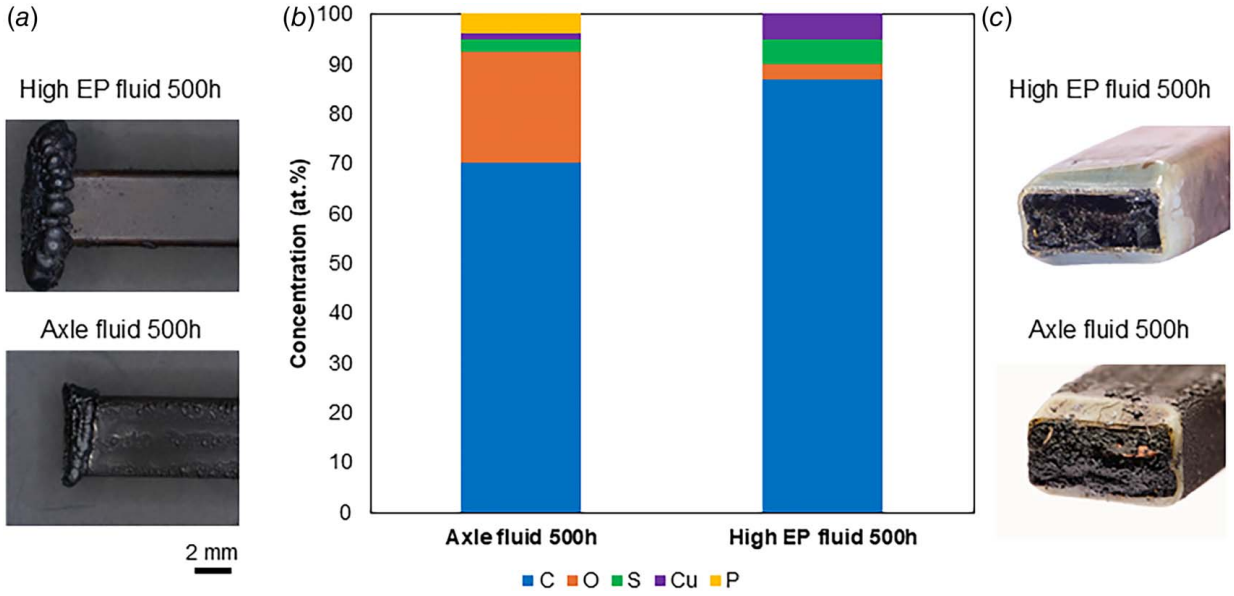

Fig. 18 Solid deposits found at the ends of wires aged in the liquid phase in high active sulfur fluid and axle fluid: (*a*) images of the deposits, (*b*) composition of the deposits measured by SEM–EDS, and (c) images of the wire after the deposit was removed

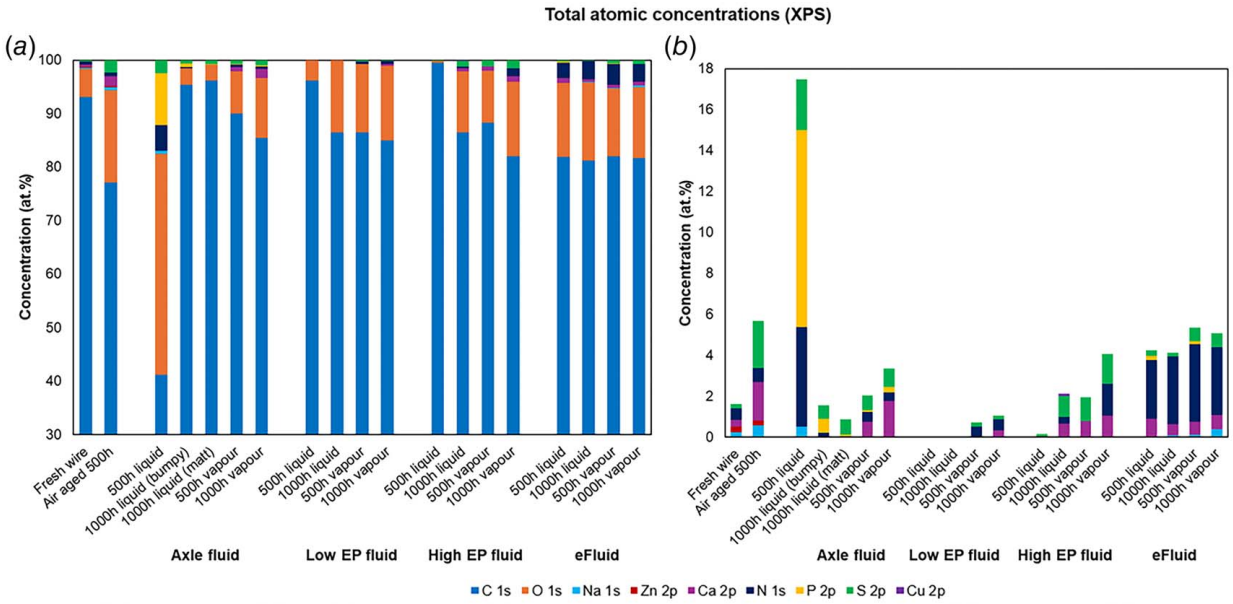

Fig. 19 Composition of the coating surface after aging in various oils, measured by XPS, showing (*a*) overall composition and (*b*) composition without carbon and oxygen allowing the other elements to be compared more easily

and 0.22–2.29% respectively), presumably due to contamination from vapors from the other test fluids. The coating remained present and >10 nm thick, since copper was not seen on any of the aged wire coating surfaces by XPS, except for 0.1% on the wire aged in high active sulfur fluid. By SEM–EDS copper was observed, due to the high penetration depth of the EDS measurement, but at low levels (<0.1%) on all wires and remaining approximately constant.

Sulfur was seen on almost all polymer surfaces by XPS, with levels up to or similar to those after aging in air for 500 h (<3%). The sulfur was present as sulfate ($2p_{3/2}$ peak position 168–169 eV) [20] in all aged wires with appreciable sulfur on the surface, originating from additives in the fluid. The two fluids containing higher active sulfur (axle fluid and high active sulfur fluid) also yielded sulfide on the coatings ($2p_{3/2}$ peak position 163–164 eV, Fig. 20) [20]. Although copper sulfide formation is expected when active sulfur reacts with copper, no copper was seen on the surface. Therefore, the coating provides suitable protection against copper sulfide formation on the surface when intact under these conditions. Note that copper sulfide may have formed at the interface between the copper and the coating due to fluid penetration into the coating.

Phosphorus was absent or in trace levels for most coatings, however the phosphorus concentrations after aging in axle fluid after 500 h were very high (9.6% by XPS). This concentration was reduced to about 0.7% after 1000 h on bumpy regions, and ~0.1% on matt regions and the vapor phase region by XPS. In all cases, the phosphorus was present in the form of phosphate

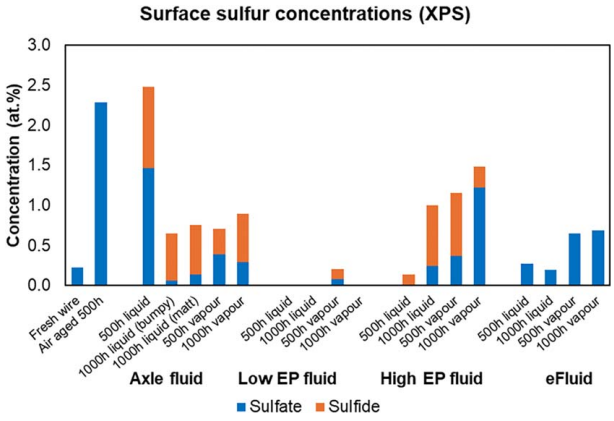

Fig. 20 Coating surface concentrations of sulfate and sulfide, measured by XPS

and/or phosphite (XPS $2p_{3/2}$ peak position ~133 eV, phosphate and phosphite have very similar binding energies around 133–134 eV) [20–22]. The axle fluid used contains high concentrations of phosphates and phosphites, which are, therefore, depositing or reacting on the polymer surface. As the aging time increases, these compounds appear to be removed from the surface, possibly dissolving back into solution, or migrating deeper into the coating. The eFluid also contains phosphorus compounds but these appear to remain in solution.

The deposit on the wire aged in axle fluid could be easily chipped off the wire coating using a diamond scribe, leaving the gray polymer coating beneath visible. The coating was seen to be intact. The deposit (after removal from the surface) was found by SEM–EDS to contain sulfur (4.7%), phosphorus (1.4%), and only low amounts of copper (0.02%) along with high concentrations of carbon, nitrogen, and oxygen (70.9%, 6.3%, and 16.6% respectively). Elsewhere, mostly notably close to the boundary between the liquid and vapor phases, the black deposit appeared uniform

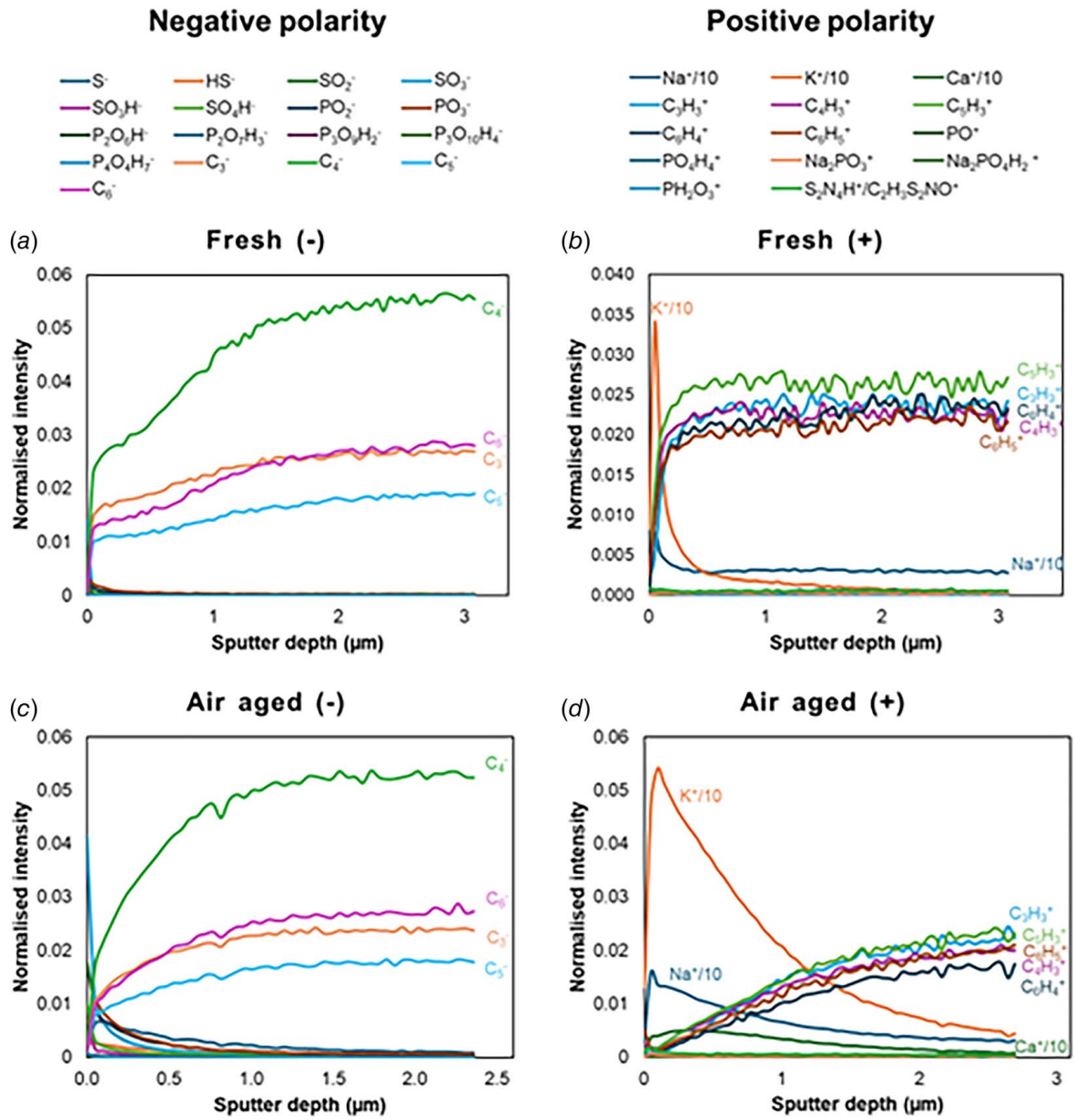

Fig. 21 TOF-SIMS depth profiles for (*a*) and (*b*) fresh; and (c) and (*d*) air-aged coated wires, showing selected ions relating to the polymer and the deposits on the surface. Intensities for Na^+, K^+, and Ca^+ have been divided by ten to keep data on a similar scale.

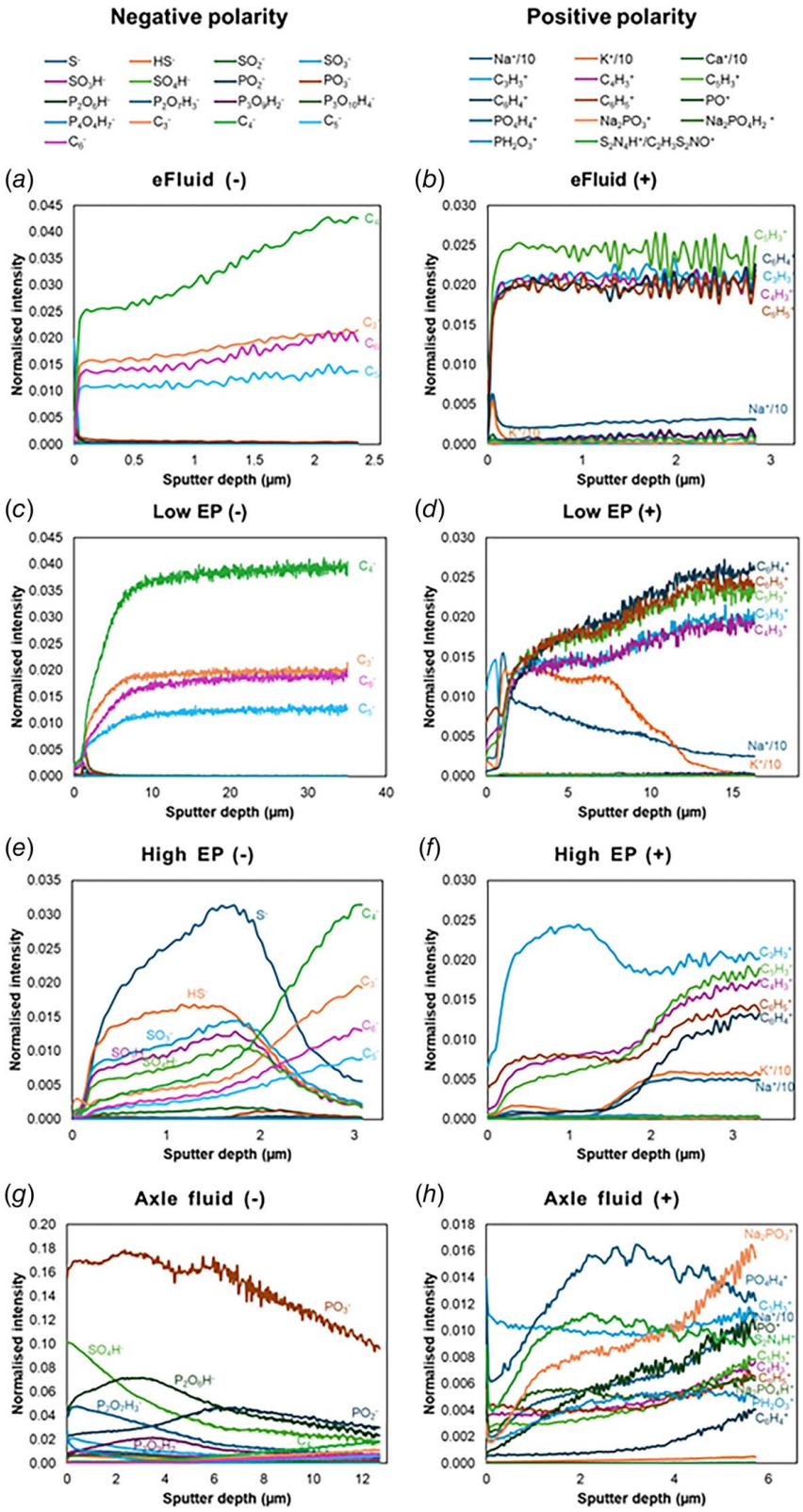

Fig. 22 TOF-SIMS depth profiles for coated wires aged in the four fluids (straight wires in the liquid phase), showing selected ions relating to the polymer and the deposits on the surface. Intensities for Na^+, K^+, and Ca^+ have been divided by ten to keep data on a similar scale.

and matt. The black deposit on the wire aged in high active sulfur fluid could also be scratched off to reveal the gray coating beneath. The deposit was found by SEM–EDS to contain sulfur (3.0%), low amounts of phosphorus, copper, and sodium (0.36%, 0.81%, and 0.55% respectively), and high amounts of carbon, nitrogen, and oxygen (73.7%, 3.2%, and 18.5% respectively), implying that these arise from decomposition of the fluid rather than corrosive processes.

Low concentrations of sodium (<0.8%) were sometimes seen, and calcium concentrations remained similar to or below those seen on air-aged wires. Nitrogen was present in reasonably high concentrations, likely from the atmosphere or oil.

The surface species on the short wires ages in the liquid phase were also measured and depth profiled using TOF-SIMS with sequential sputtering steps (Figs. 21 and 22), for the wires aged for 500 h. Ions likely arising from the polymer consisting of carbon and hydrocarbons were tracked, alongside a selection of phosphate, phosphite, sulfate, and sulfide ions. Note that only the ions with higher signals were selected to display the changes among different samples. The trends for $C_{10}H_6O_3^+$, $C_{10}H_8O_3^+$, $C_{14}H_4O^+$, $C_{12}H_8O_3^+$, $C_{12}H_{10}O_3^+$, $C_{15}H_{11}O_3^+$ follow the same pattern as $C_3H_3^+$, $C_4H_3^+$, $C_5H_3^+$ in all cases, so are excluded for brevity.

For the fresh and air-aged samples, the spectra looked similar throughout the depth profile. The expected polymer ions reached a steady intensity by around 2.2 μm depth (Fig. 21). Prior to this time, the species seen were primarily fatty acids and some metal ions (Na^+, K^+, Ca^+), likely arising from surface contamination due to sample manufacture and handling. The eFluid sample showed similar spectra and contamination to the fresh and air-aged samples (Figs. 22(*a*) and 22(*b*)), reaching a similar profile of polymer ions after around 2.2 μm again, showing that there is no sulfide, sulfate, phosphite, or phosphate forming a coating on the surface.

For the low active sulfur fluid, the bulk polymer was again reached after around 2.2 μm sputter depth (Figs. 22(*c*) and 22(*d*)). Prior to this depth, high concentrations of Na^+ and K^+ were seen on the surface. For the high active sulfur fluid, the bulk polymer was almost reached after around 3.3 μm sputter depth (Figs. 22(*e*) and 22(*f*)). Prior to this depth, high concentrations of sulfides and sulfates were seen on the surface, in agreement with the XPS results. In the axle fluid, the polymer ion intensity remained low even after 11 μm (Figs. 22(*g*) and 22(*h*)). High intensities of phosphates and phosphites were seen throughout, decreasing in intensity after around 6.6 μm. Sulfates were also seen close to the surface with intensities then decreasing. The bulk polymer was not reached in this experiment, indicating that the surface layer is thicker on this sample than 13.2 μm.

Overall, the polymer coatings were found to be intact after aging in all fluids. In the fluids with higher active sulfur, black deposits were found on the surface, which were conductive in some areas. These areas correspond with higher surface sulfur including sulfides, and, in the case of the axle fluid, phosphates, and/or phosphites. The deposits could be scratched off the surface, revealing an intact polymer coating beneath, which continues to protect the copper wire against corrosion.

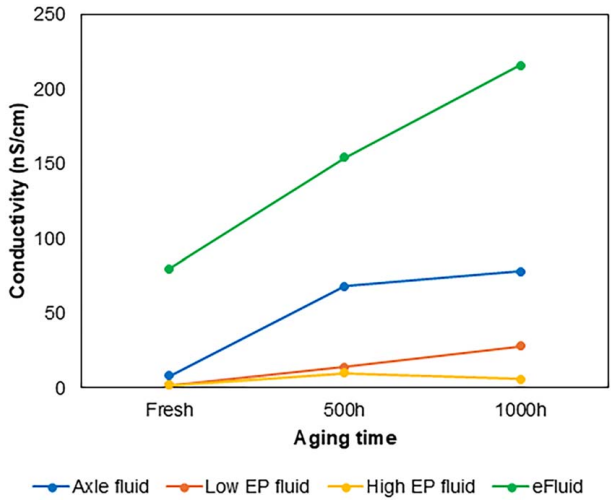

Fig. 23 Conductivity of the fluids after aging with bent wires partially immersed

3.2.3.5 Analysis of fluids. Analyzing the fluids used post-test, only low concentrations of copper were found (up to 2 mg/l). Copper was only found when there was copper exposed in the fluid and for the fluids lowest in sulfur. Copper was, therefore, not lost from the wire except in the form of solid deposits remaining on the wire or coating. Concentrations of elements from additives from the fluid (calcium, boron, phosphorus, and sulfur) remained similar except in a few cases: the sulfur levels in the high active sulfur fluid decreased dramatically, presumably to form the deposit seen on the wire/polymer coating, while sulfur levels in the axle fluid remained unchanged but phosphorus and boron levels decreased dramatically, presumably migrating to the surface of the wire/polymer coating or evaporating.

The conductivity of the fluids typically increased during the test (Fig. 23, measured only on the fluids aged with bent wires). Lubricant formulations can degrade at high temperatures, producing small polar molecules which increase the conductivity of the fluid. Whilst there are measurable differences between the aged fluids, the conductivity of these fluids is still in the static dissipative region and would not be considered conductive [23].

4 Conclusions

Through the analysis of electric machines, we observed the presence of copper sulfide specifically in machines exposed to transmission and/or axle oils. These sulfides, known for their conductive properties, were found on machines that experienced failures. Coating aging experiments indicated the formation of conductive films on the polymer layer by axle oil and fluids with high sulfur concentrations. This is notable as these chemicals typically adhere to polar surfaces but seem to form films on non-polar polymer surfaces, potentially compromising the insulation properties if there are cracks or imperfections present.

The effect of this phenomenon appears to be influenced by the type of chemistry involved, with sulfur and phosphor-based ions detected, and by the treatment rate, as fluids with lower active sulfur levels behaved differently compared to those with higher levels. Oil conductivity measurements before and after aging showed minimal changes, remaining within the static dissipative regime. Contaminations with elements typically found in transmission and axle oils were identified in eMachines that reported short circuits and damage, whereas no such contaminations were found in eMachines without failures. TOF-SIMS analysis confirmed the formation of copper sulfide clusters, $Cux S_y$, on the failed eMachines.

Activation energy experiments confirmed that copper sulfide formation can occur at normal eMachine operating temperatures, with the rate of reactions suggesting damage within a timeframe of 10–100 days, depending on the specific temperatures and utilization of the vehicle. These findings elucidate the behavior of copper sulfide and the risks posed by certain oils in eMachines. The formation of hollow regions under the coating due to copper corrosion is significant, as these hollow regions between the insulation and conductive parts are sufficient to cause electrical failure.

Further research is needed to develop strategies to mitigate these risks and ensure the long-term reliability of eMachine coatings. This includes exploring new materials and coatings that can resist corrosive sulfur compounds and improving maintenance practices to detect and address potential issues early.

Acknowledgment

The authors thank the Lubrizol Corporation and Scania CV AB for supporting the publication of this work. Thank you to Aimee Collins for supporting sample preparation. The authors thank the Nanoscale and Microscale Research Centre, UK (nmRC) for

providing access to XPS and TOF-SIMS instrumentation and Dr. Hannah Constantin for technical assistance. The authors thank Peter Sjövall and Illia Dobryden at Research Institutes of Sweden (RISE) for providing the analysis with TOF-SIMS and technical assessments.

Conflict of Interest

There are no conflicts of interest.

Data Availability Statement

The datasets generated and supporting the findings of this article are obtainable from the corresponding author upon reasonable request.

References

[1] Beyer, M., Brown, G., Gahagan, M., Higuchi, T., Hunt, G., Huston, M., Jayne, D., et al., 2019, "Lubricant Concepts for Electrified Vehicle Transmissions and Axles," Tribol. Online, **14**(5), pp. 428–437.
[2] Newcomb, T., 2023, "A Brief Review of the Rapid Transformation of Driveline Lubricants for Hybrid Electric and Electric Vehicles," Front. Mech. Eng., **9**(1), pp. 1–5.
[3] Rudnick, L. R., 2009, *Lubricant Additives: Chemistry and Applications*, CRC Press, Boca Raton, FL, pp. 477–498.
[4] Papay, A. G., 2006, "Antiwear and Extreme-Pressure Additives in Lubricants," Lubr. Sci., **10**(3), pp. 209–224.
[5] Hunt, G. J., Gahagan, M. P., and Peplow, M. A., 2023, "The Influence of Model Organosulfur Extreme Pressure Additives and Analogues on the Corrosion of Copper as Measured by a Wire Corrosion Test Method," Lubr. Sci., **35**(3), pp. 155–162.
[6] Nyman, P., Hunt, G., Forslund, M., and Björklund, P., 2022, "Towards a Common Test Method for Corrosion in EMotors," CTI Symposium, Germany, July 12.
[7] Hunt, G., and Prengaman, C., 2020, Understanding Vapor and Solution Phase Corrosion of Lubricants Used in Electrified Transmissions. *SAE Technical Paper Series*.
[8] Grozdanov, I., and Najdoski, M., 1995, "Optical and Electrical Properties of Copper Sulfide Films of Variable Composition," J. Solid State Chem., **114**(2), pp. 469–475.
[9] Okamoto, K., and Kawai, S., 1973, "Electrical Conduction and Phase Transition of Copper Sulfides," Jpn. J. Appl. Phys., **12**(8), pp. 1130–1138.
[10] Hunt, G. J., Gahagan, M. P., and Peplow, M. A., 2017, "Wire Resistance Method for Measuring the Corrosion of Copper by Lubricating Fluids," Lubr. Sci., **29**(4), pp. 279–290.
[11] Bares, J., Hunt, G., Prengaman, C., Wicks, J., and Nicholson, S., 2020, "Establishing Long-Term Corrosion Protection of Copper-Based Alloys in Modern Transmissions," SAE Int. J. Fuels Lubr., **13**(3), pp. 251–264.
[12] Arrhenius, S., 1889, "Über die Reaktionsgeschwindigkeit bei der Inversion von Rohrzucker durch Säuren," Z. Phys. Chem., **4**(1), pp. 226–248.
[13] Lente, G., Fábián, I., and Poë, A. J., 2005, "A Common Misconception About the Eyring Equation," New J. Chem., **29**(6), pp. 759–760.
[14] Eyring, H., 1935, "The Activated Complex in Chemical Reactions," J. Chem. Phys., **3**(2), pp. 107–115.
[15] Hunt, G. J., Choo, L., and Newcomb, T., 2023, 100 Years of Corrosion Testing—Is It Time to Move beyond the ASTM D130? The Wire Corrosion and Conductive Deposit Tests.
[16] Hunt, G. J., Javaid, R., Simon, J., Peplow, M., and Prengaman, C., 2022, Understanding Conductive Layer Deposits: Test Method Development for Lubricant Performance Testing for Hybrid and Electric Vehicle Applications.
[17] Industries, A. C. E., 2000, *IPC-TM-650 Test Methods Manual*, IPC, Bannockburn, IL, p. 4.
[18] Fairley, N., Fernandez, V., Richard-Plouet, M., Guillot-Deudon, C., Walton, J., Smith, E., Flahaut, D., et al., 2021, "Systematic and Collaborative Approach to Problem Solving Using X-ray Photoelectron Spectroscopy," Appl. Surf. Sci. Adv., **5**, p. 100112.
[19] Rönnhult, T., Brox, B., and Fritze, G., 1987, "The Influence of Surface Topography on the X-ray Intensity in Electron Microprobe Analysis (EDS/WDS)," Scanning, **9**(2), pp. 81–87.
[20] Moulder, J. F., Stickle, W. F., Sobol, P. E., and Bomben, K. D., 1992, *Handbook of X-ray Photoelectron Spectroscopy*, Perkin-Elmer Corporation, Eden Prairie, MN.
[21] Barros-Bouchet, M. I. D., Righi, M. C., Philippon, D., Mambingo-Doumbe, S., Le-Mogne, T., Martina, J. M., and Bouffet, A., 2015, "Tribochemistry of Phosphorus Additives: Experiments and First-Principles Calculations," RSC Adv., **5**, p. 49670.
[22] Bertrand, P. A., 1982, "XPS Study of Chemically Etched GaAs and InP," J. Vac. Sci. Technol., **18**(1), pp. 28–33.
[23] McFadden, C., Hughes, K., Raser, L., and Newcomb, T., 2016, "Electrical Conductivity of New and Used Automatic Transmission Fluids," SAE Int. J. Fuels Lubr., **9**(3), pp. 519–526.